Draft Version

Calculation of Binding Affinities for Thiadiazole Urea Inhibitors with Matrix Metalloproteinases from Molecular Modeling Calculations

Robert C. Rizzo, Samuel Toba, and Irwin D. Kuntz*

Contribution from the Department of Pharmaceutical Chemistry, University of California at San Francisco, San Francisco, California 94143-2240. Date Received April 18, 2005

Introduction

Matrix metalloproteinases (MMPs) are zinc dependent enzymes involved in a multitude of physiological processes including embryonic development, wound repair, and tissue remodeling.[1-4] Specific MMPs target the extracellular matrix (ECM) for degradation and promote the formation of new blood vessels (angiogenesis).[1] Given that angiogenesis is essential for the development and progression of tumor growth, MMP inhibitors could serve as effective anti-cancer agents.[1-3] However, despite the initial excitement offered by first generation MMP inhibitors to restrict invasive tumor growth and metastasis in a variety of animal models,[4,5] clinical trial results have been disappointing; no clinical efficacy in humans has been demonstrated.[2,5] Recent studies have shown that MMPs also appear to regulate the production of angiostatin, a potent angiogenesis inhibitor that inhibits tumor growth.[1,2,6,7] These findings suggest that more selective MMP inhibitors are crucial for the development of clinically effective chemotherapeutics.[1,8,9]

Several classes of compounds have been reported which bind to the active site residues in MMPs and effectively prevent normal substrate degradation. Compounds include peptidomimetic, nonpeptidomimetic, tetracycline, and bisphosphonate

inhibitors.[4,10] Peptidomimetics were originally designed based on the amino acid sequence flanking the cleavage site in the natural substrate, collagen, for the MMP collagenase. Several nonpeptidomimetics have been guided through structure-based design[11] approaches using crystallographic information.[4,10] Structural studies have revealed that most inhibitors interact with MMP active site residues through an elaborate hydrogen-bond network and chelation of the active-site zinc (Figure 1).[4]

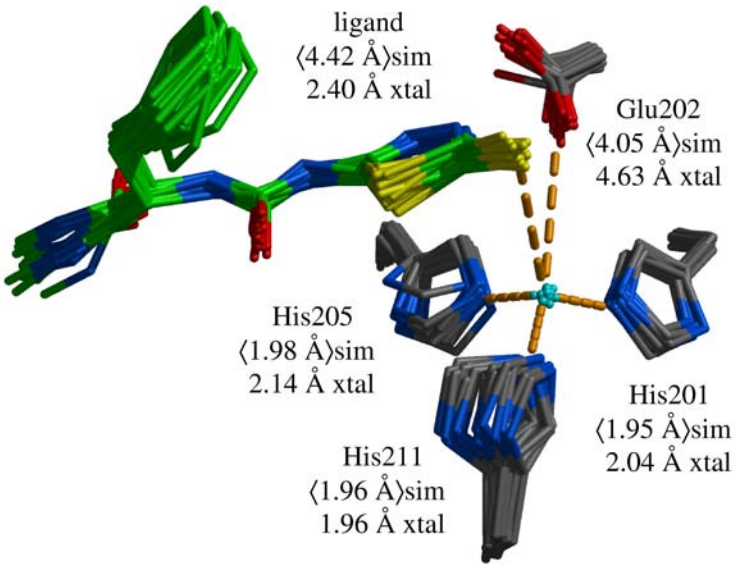

Figure 1. Chelation of the active-site zinc ion by thiadiazoles. Ligand **46** with stromelysin-1 (pdb entry 1USN) from 20 ps of a GB-MD simulations. Inhibitor in green, protein residues in CPK colors, and catalytic zinc in cyan.

Several zinc binding groups (ZBG) have been discovered which include a carboxylate, aminocarboxylate, sulfhydryl, hydroxamate, phosphonate, or phosphinate moiety.[4,10] Recently, 5-substituted-1,3,4-thiadozole-2-thione compounds have been reported that

contain a novel ZBG where coordination occurs through the exocyclic sulfur of a thiadiazole group.[12] Structure-activity-relationship (SAR) studies have shown that thiadiazoles are selective for stromelysin-1 (MMP-3) over gelatinase-A (MMP-2) with little or no affinity for collagenase (MMP-1).[12]

The dual roles that matrix metalloproteinases appear to play in cancer growth and metastasis[1,5] highlight the need for studies that address a physical basis for selective inhibition of specific MMPs. In this report we have used computational modeling techniques to develop, refine, and validate simulation protocols and methods that can be used in the design of anti-cancer agents targeting the MMPs. We have focused on two specific MMPs, stromelysin-1 and gelatinase-A, since both have been implicated in breast cancer,[13,14] crystallographic structures of protein-ligand complexes are available,[15,16] and structure-activity data have been reported.[12] Although many MMPs are over-expressed in breast cancer tissue and tumor cell lines,[13,14] stromelysin-1, in particular, has been shown to promote mammary carcinogenesis in mice[17,18]

Computer simulations of 5-substituted-1,3,4- thiadiazole -2-thiones (Table 1) with both stromelysin-1 and gelatinase-A have been performed in order to estimate free energies of binding for comparison with experiment. Aims of this research include: (1) the development of generalized protocols and methods for continuum-based computer simulations (no explicit water) for systems with metallo centers, (2) the accurate prediction binding affinities and selectivities of thiadiazole inhibitors with MMPs in comparison with experimental data, and (3) the elucidation of the basis for selectivity between MMPs through interpretation of the structural and energetic results from the

simulations. By accurately modeling known MMP-ligand systems, new, selective, and potent MMP inhibitors can be proposed with greater confidence.

Table 1. Inhibition of stromelysin-1 (str) and gelatinase-A (gel) by thiadiazole ureas. K_i values in μM. [a]Estimated experimental binding energies $\Delta G_{exptl} \approx RT \ln (K_i)$ in kcal/mol.

No.	Structure	str K_i	gel K_i	str ΔG_{bind} exptl	gel ΔG_{bind} exptl
70	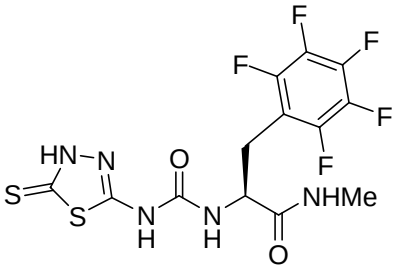 PNU-142372	0.018	3.0	–10.99	–7.84
46	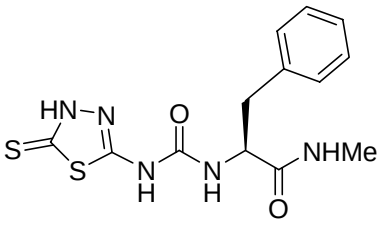 PNU-107859	0.71	31	–8.73	–6.40
57	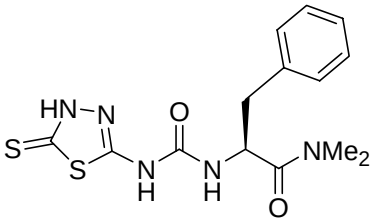	2.3	226	–8.00	–5.17
56	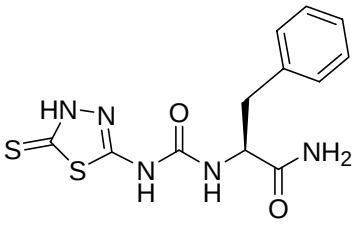	3.3	>200	–7.78	>–5.25
29a	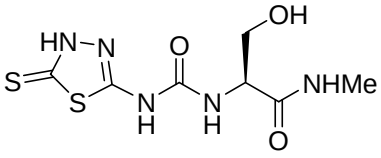	31	>200	–6.40	>–5.25

45	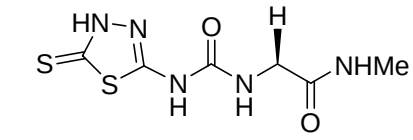	166	>100	−5.36	>−5.68

[a]Reference 12.

Theoretical Methods

Structure-based drug design using computational methods continues to hold great promise as simulation methods and protocols become more refined and computers become more powerful. Of particular interest are simulation methods that accurately estimate free energies of binding (ΔG_{bind}) between small drug-like molecules and a target protein without resorting to more rigorous and very CPU intensive methods of free energy perturbation (FEP) and thermodynamic integration (TI) techniques.[19] The recently reported MM-PBSA method[20-22] is faster by at least a factor of 10 than more traditional FEP or TI techniques and does not require any experimental data or fitting of parameters as in the Åqvist linear response (LR)[23] and extended linear response (ELR)[24-27] simulation methods. MM-PBSA is easily applicable to a wide range of diverse ligands.

In the original MM-PBSA formalism,[21,22] the total free energy of the system (G) is computed according to eq 1.

$$G = G_{polar} + G_{nonpolar} + E_{mm} - TS \quad (1)$$

Here, a polar solvation energy term G_{polar} is computed in continuum solvent using a finite Poisson-Boltzmann (PB) model and a nonpolar solvation energy term $G_{nonpolar}$ is computed from a solvent-accessible surface area (SASA) calculation using eq 2 for each isolated state (receptor, ligand, or complex).[21,22]

$$G_{nonpolar} = (0.00542 * SASA) + 0.92 \quad (2)$$

Alternatively, a Generalized Born (GB) model may be used to estimate $G_{polar,}$ yielding a method called MM-GBSA.[22] The E_{mm} term in eq 1 is a sum of the electrostatic (Coulombic), van der Waals (Lennard-Jones) and internal energies (bonds, angles, and dihedrals). Entropic effects may be included (TS term) where T is the temperature and the entropy S is typically estimated based on classical statistical formulas and normal-mode analysis of representative snapshots of energy-minimized structures from a molecular dynamics (MD) trajectory. The binding free energy is then estimated from eq 3.[21,22]

$$\Delta G_{bind} = G_{complex} - (G_{protein} + G_{ligand}) \quad (3)$$

A MD simulation with explicit solvent is typically performed for each ligand bound to the protein to yield snapshots containing representative structures of the system(s),[21,22,28-34] although in the present research no explicit water was used in the simulation. Free energies (G), for each species, complex, protein, and ligand, are estimated with eq 1 using a set of Cartesian coordinates from a given trajectory snapshot and the difference (eq 3) gives ΔG_{bind}. Multiple snapshots are taken during the course of the MD trajectory to yield an average ΔG_{bind}. For $G_{complex}$, bulk explicit solvent (if present) is removed, while for $G_{protein}$ and G_{ligand} explicit solvent and the ligand or the protein are removed respectively.[21,22] Specific individual water molecules suggested to be important for ligand recognition may be retained in the coordinate files used in the post-trajectory analysis.[31]

Computational Details

System Setups. Crystallographic structures of stromelysin-1 (pdb entry 1USN)[15] complexed with a thiadiazole inhibitor PNU-107859 (Table 1, compound **46**) and gelatinase-A (pdb entry 1QIB)[16] complexed with a hydroxamate inhibitor were used as starting coordinates for the present simulations. No crystallographic structure of gelatinase-A complexed with a thiadiazole inhibitor is currently available. Five analogs of compound **46** were manually constructed using the crystallographic coordinates of the stromelysin-1 complex (1USN) as a guide with the MOE program.[35] Analogs **70, 57, 56, 29a,** and **45** from Jacobsen et al.[12] were chosen to (1) provide a reasonable range of experimental free energies of binding (Table 1) for comparison with experiment, and (2) be structurally similar to or smaller than the parent compound **46**. Using structurally similar compounds facilitates the construction of each protein-ligand complex and helps ensure that the ligands are placed in a reasonable starting conformation.

Figure 2 (right) highlights the gross structural similarity between the stromelysin-1 (green tube) and gelatinase-A (blue tube) enzymes, especially in the vicinity of bound ligand PNU-107859 (red) and the coordinated zinc ion (magenta); a molecular surface representation of stromelysin-1 is also shown (left).

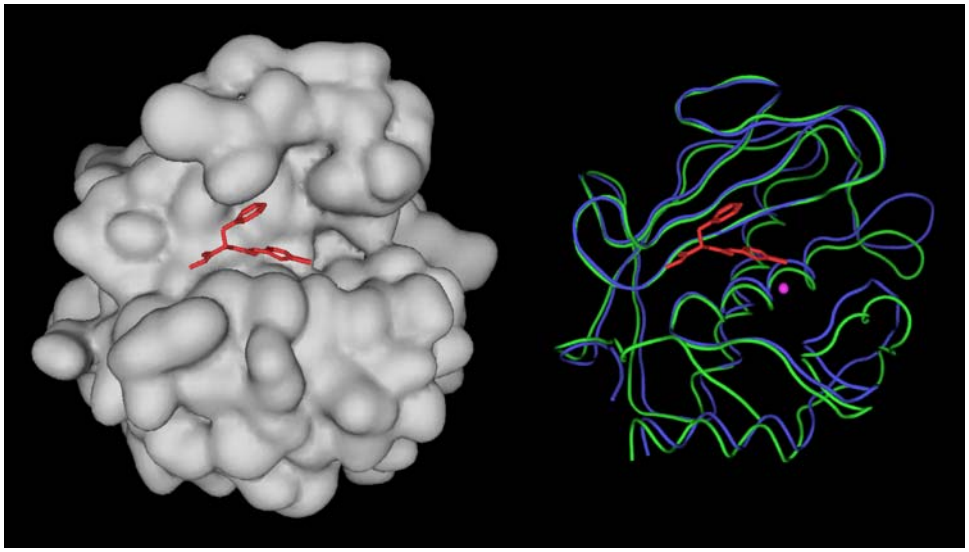

Figure 2. Left: Molecular surface of stromelysin-1 in gray showing ligand **46** in red. Right: Overlay of stromelysin-1 (green tube, pdb entry 1USN) and gelatinase-A (blue tube, pdb entry 1QIB) showing ligand **46** (red) and coordinated catalytic zinc ion (magenta). The two proteins were aligned using C_α carbons from residues 164-170 and 194-206 (0.17 Å rmsd difference).

Standard PARM99[36] force field parameters were assigned to the protein, augmented by the Stote et al. nonbonded zinc model ($q = +2\ e^-$, $\sigma = 1.7$ Å, $\varepsilon = 0.67$ kcal/mol),[37] using the LEAP program in AMBER7.[38] The Stote model was shown to yield the best overall results out of eight zinc parameter sets tested for docking ligands to thermolysin[39] and, more recently, MM-PBSA calculations have used the nonbonded model to rank binding energies for six known carboxylate ligands of stromelysin-1 in reasonable agreement with experiment.[28] For the ligands, GAFF[38] force fields parameters and AM1-BCC[40,41] partial charges were assigned using the

ANTECHAMBER program as implemented in AMBER7.[38] Using this procedure, twelve simulation-ready systems were constructed each containing one of six ligands, that only differed in initial receptor (stromelysin-1 or gelatinase-A) coordinates.

Generalized Born Molecular Dynamics Simulations (GB-MD). A two-stage conjugant gradient energy minimization protocol was applied to each protein-ligand complex prior to the MD simulations. First, a minimization was performed for each system in which only the receptor heavy atoms were restrained to their crystallographic positions using a harmonic potential (force constant = 1000.0 kcal/mol Å^2). A second restrained minimization was then performed using a much weaker force constant = 5.0 kcal/mol Å^2 in which atoms designated as AMBER type main-tree were restrained. Both minimizations employed a distance dependant dielectric constant (4r) and loose tolerance for convergence (drms=0.1 kcal/mol Å).

After the minimizations, molecular dynamics simulations were initiated without explicit water using the pairwise GB continuum solvent model of Hawkins and coworkers[42,43] implemented in the SANDER module of AMBER7. Simulations employed a 1 femtosecond time step for 40010 steps corresponding to a total of 40.01 picoseconds of GB-MD. The final desired temperature of 298 K was obtained by requesting a heating cycle from 0 to 298 K over the course of the first 5000 MD steps with temperature regulation maintained via coupling to an external heat bath using the Berendsen scheme[44] and a coupling time constant tautp = 1.0 ps. Main-tree type atoms were lightly restrained using a weak harmonic force constant = 5.0 kcal/mol Å^2 and the SHAKE[45] algorithm was applied to constrain bonds involving hydrogen atoms.

Dielectric constants of 1 (interior) and 80 (exterior) were employed in all GB-MD simulations.

MM-GBSA Processing. Following the extraction of coordinates representing individual species (complex, receptor, or ligand), from the GB-MD trajectory of each protein-ligand complex, the various MM-PB/GBSA energy terms in eq 1 were computed as follows. Electrostatic (E_{coul}), van der Waals (E_{vdw}), and internal energies were obtained using the SANDER module in AMBER7. Polar energies (G_{polar}) were obtained from the DelPhi[46] (PB energies), and AMBER7[38] (GB energies) programs using dielectric constants of 1 and 80 to represent gas and water-phases respectively. For the PB and GB calculations the same coordinates, charges, and radii (mbondi)[47] were used. Nonpolar energies ($G_{nonpolar}$) were determined from eq 2 using SASAs computed with the MOLSURF[38] program.

Results and Discussion

Continuum Trajectory Stability. To gauge whether the GB-MD simulations were stable and converged, energetic and structural properties were monitored during the course of the trajectories as illustrated in Figure 3 for compound **46** with stromelysin-1. In Figure 3, despite the short simulation times, instantaneous properties appear to be well converged before the final data collection phase at 20.01 ps. Standard errors of the mean (sem) for ligand **46** with stromelysin-1 computed from the last 201 snapshots are low; $\Delta G_{MM\text{-}GBSA}$ = 0.13 kcal/mol, Temp = 0.25 K (Figure 3a), ΔE_{vdw} = 0.13 kcal/mol, ΔE_{coul} = 0.25 kcal/mol, ΔG_{polar} = 0.21 kcal/mol, and $\Delta G_{nonpolar}$ = 0.005 kcal/mol (Figure 3b).

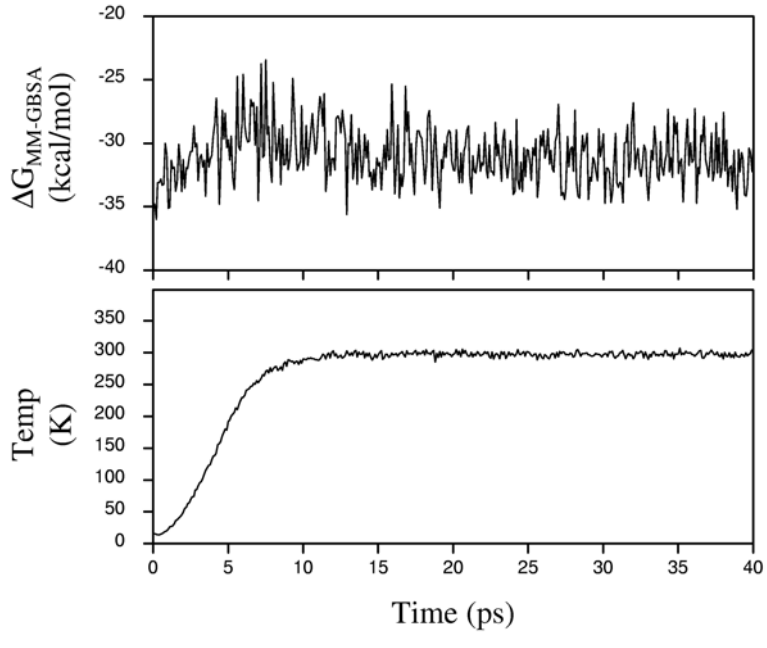

(a)

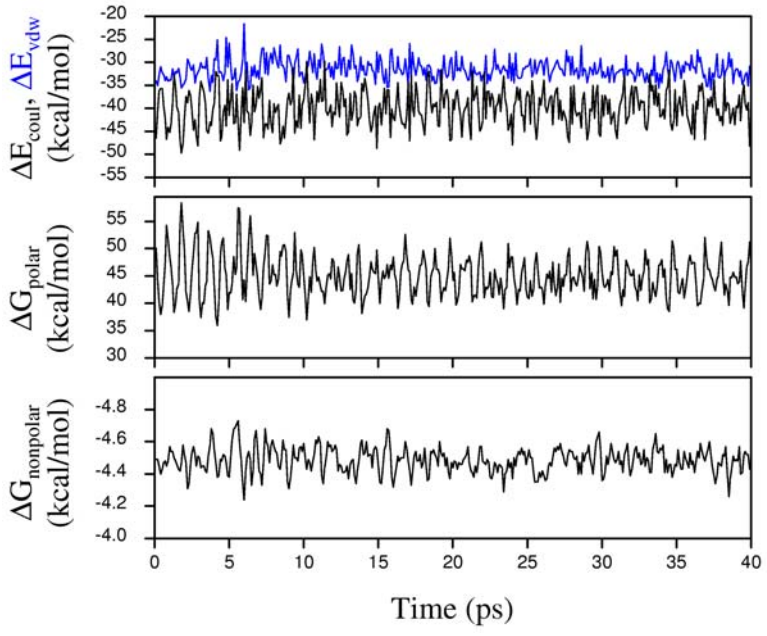

(b)

Figure 3. Instantaneous results from GB-MD simulations of ligand **46** with stromelysin-1 plotted vs. time. (a) Temperature in Kelvin and $\Delta G_{MM\text{-}GBSA}$ sum (ΔE_{vdw} + ΔE_{coul} + ΔG_{polar} + $\Delta G_{nonpolar}$) in kcal/mol, (b) individual components ΔE_{vdw}, ΔE_{coul}, ΔG_{polar}, $\Delta G_{nonpolar}$ in kcal/mol.

Stromelysin-1 Binding. Free energies of binding were computed for stromelysin-1 (eqs 1 and 3) from snapshots saved every 0.10 ps from the final 20.01 ps of the GB-MD trajectories. For simulation results that include solute entropies ($\Delta G_{MM\text{-}GBSA+E}$), the best-fit line to the stromelysin-1 data yields a strong correlation coefficient with experiment (r^2 = 0.97), low standard deviation of 1.02 kcal/mol, and average unsigned error of only 0.79 kcal/mol (Figure 4). The excellent correlation with experiment is especially encouraging given the challenges presented; simulations are continuum-based, contain a metallo center, and are short (40.01 ps) by conventional standards.

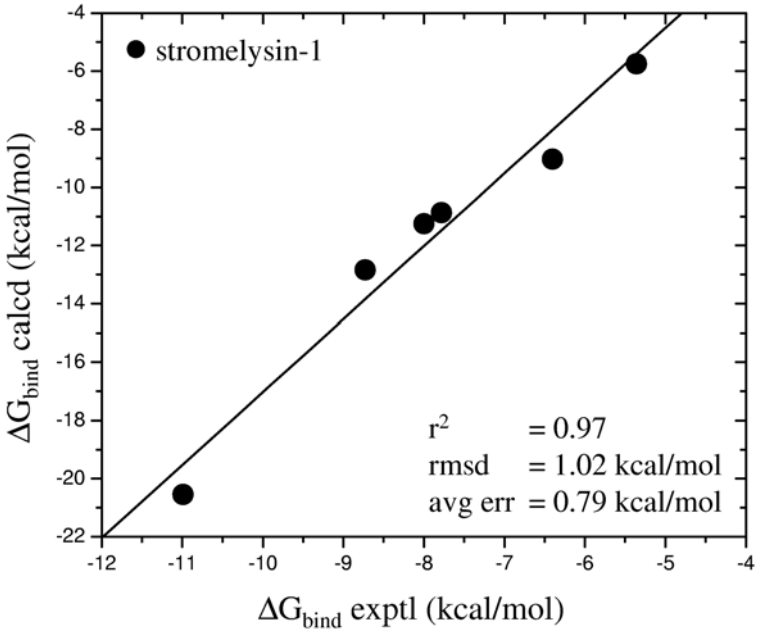

Figure 4. Predicted free energies of binding (ΔG_{bind} calcd) computed using eqs 1 and 3 from MM-GBSA calculations vs. experiment (ΔG_{bind} exptl) for six ligands with stromelysin-1(●).

During the course of the GB-MD simulations, the ΔE_{coul} and ΔG_{hyd} (ΔG_{polar} + $\Delta G_{nonpolar}$) energies are highly anti-correlated ($r = -0.78$, $r^2 = 0.61$) as illustrated in Figure 5 for ligand **46**. As expected, favorable protein-ligand electrostatic energies (ΔE_{coul}) are approximately equal but opposite in sign to the desolvation penalties (ΔG_{hyd}) at each point in the GB-MD trajectory. The two competing effects nearly sum to zero and the instantaneous free energies of binding are then dominated by the favorable ΔE_{vdw} and unfavorable $T\Delta S$ terms. Remarkably, small differences in any average term can then account for the observed variation in binding, despite the fact that fluctuations in any given term may be large.

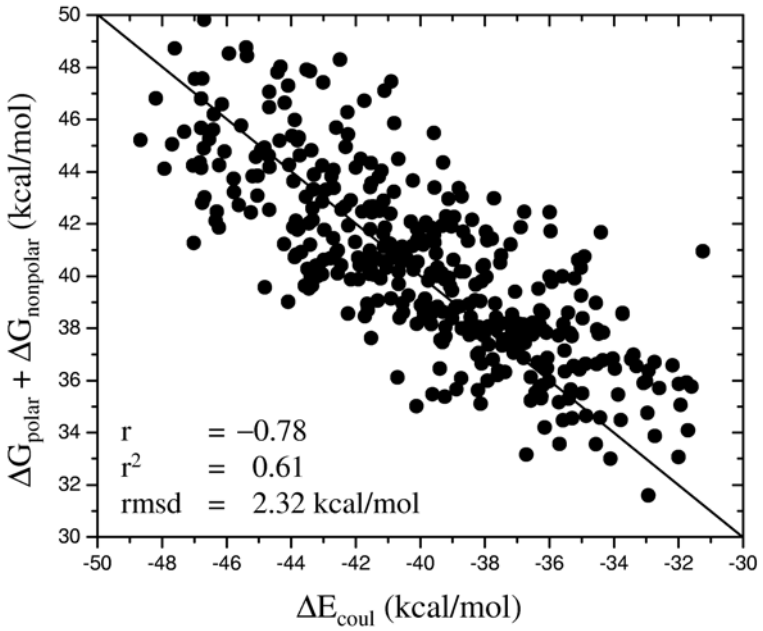

Figure 5. Protein-ligand intermolecular coulombic energies (ΔE_{coul}) vs. opposing desolvation penalties ($\Delta G_{polar} + \Delta G_{nonpolar}$) for ligand **46** with stromelysin-1. Each point

represents the energy obtained from 1 of 202 individual snapshots during the course of the GB-MD simulation.

Selectivity: Stromelysin-1 versus Gelatinase-A. Experimentally the thiadiazoles are selective for stromelysin-1 over gelatinase-A (Table 1).[12] To understand the basis for this selectivity, free energies of binding were estimated for the six ligands with gelatinase-A adopting the same MM-GBSA and normal mode protocols as in the stromelysin-1 simulations (Figure 6). Figure 8 shows the best fit line to the stromelysin-1 and gelatinase-A $\Delta G_{MM\text{-}GBSA+E}$ free energies which yield a strong correlation coefficient with experiment $r^2 = 0.71$, standard deviation = 3.33 kcal/mol, and average unsigned error = 2.46 kcal/mol.

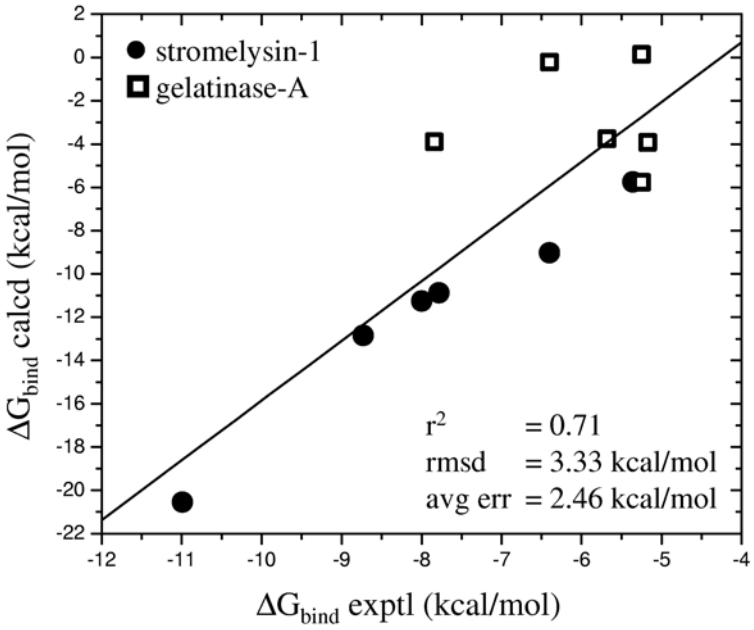

Figure 6. Predicted free energies of binding (ΔG_{bind} calcd) computed using eqs 1 and 3 from MM-GBSA calculations vs. experiment (ΔG_{bind} exptl) for the six ligands with stromelysin-1 (●) and gelatinase-A (◘).

In each case, the simulation results correctly predict that a given ligand will bind more tightly to stromelysin-1 than gelatinase-A (Figure 6), although, unlike the stromelysin-1 results, correlation with the gelatinase-A experimental data alone is reduced (Figure 6, open squares). This might be a consequence of the fact that for ligands **56**, **29a**, and **45** with gelatinase-A (Table 1) there is uncertainty in the experimental measurements, and a comparison between best and worst binders shows a compressed experimental range for the ligands with gelatinase-A (–2.59 kcal/mol) compared to stromelysin-1 (–5.63 kcal/mol). A small data range can make linear correlations of computer simulation results with experiment more difficult.[24]

Binding Site Differences. Figure 7 shows the alignment from stromelysin-1 (pdb entry 1USN) and gelatinase-A (pdb entry 1QIB) sequences obtained using the ClustalW program[48] and depicted using the BOXSHADE program.[49] The alignment highlights the overall sequence similarity, especially for residues that make contact with thiadiazole ligands (black circles •). Binding site residues are defined as being within approximately 5 Å from any ligand atom.

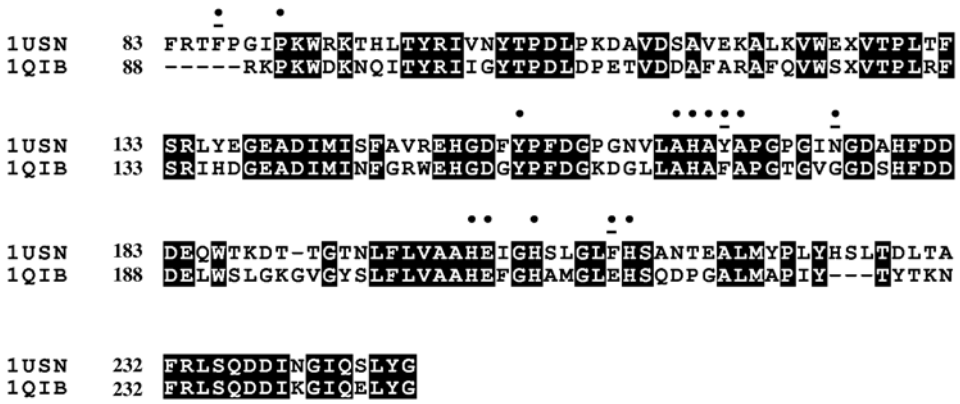

Figure 7. Stromelysin-1 (pdb entry 1USN) and gelatinase-A (pdb entry 1QIB) sequence alignment showing identical residues in black. The sequences were aligned using the ClustalW program[48] and the picture was generated using the BOXSHADE program.[49] Residues within approximately 5 Å from the ligands are marked with a black circle (•). Sequence changes in binding site residues between the two MMPs are indicated with an underlined black circle ($\underline{\bullet}$).

Of the fourteen binding site residues highlighted in Figure 7, only four sequence changes are observed (underlined black circles $\underline{\bullet}$). These four sequence changes, when coupled with structural information, can be used to interpret the experimental and computational results as illustrated in Figure 8. In Figure 8, three aromatic rings in stromelysin-1 make significant contact with the ligand compared with only one in the gelatinase-A structures. The large changes at position Phe86 (absent in gelatinase-A) and Phe210 (Glu in gelatinase-A) are expected to account for the reduction in favorable ΔE_{vdw} energies computed for the ligands with gelatinase-A compared to stromelysin-1 and probably contribute to the observed selectivity.

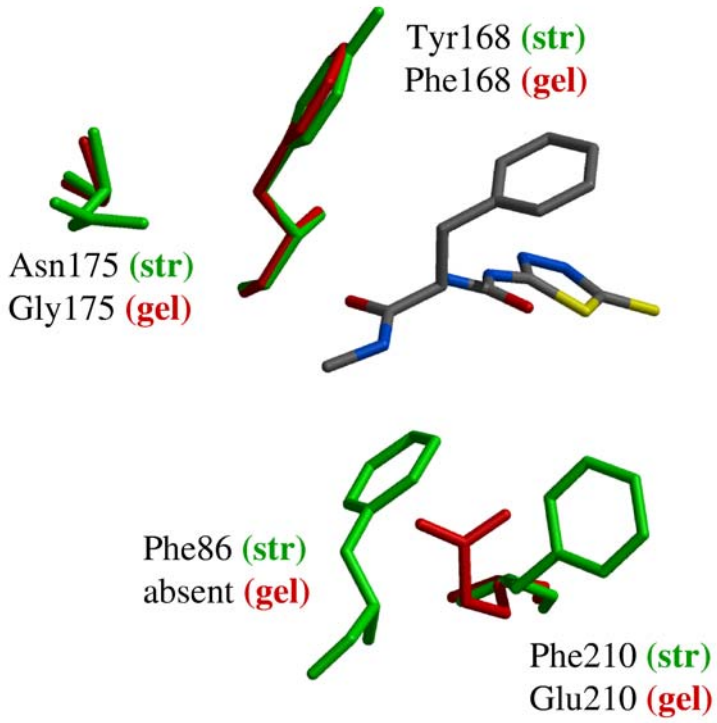

Figure 8. Binding site structural differences between stromelysin-1 (str, green) and gelatinase-A (gel, red). Ligand **46** in CPK colors, receptor and ligand coordinates from pdb entries 1USN and 1QIB aligned using C_α carbons from residues 164-170 and 194-206 (0.17 Å rmsd difference).

In the gelatinase-A structure, the void created by the absence of residue 86 is partially filled by placement of a glutamate residue midway between the positions originally occupied by Phe aromatic rings in the stromelysin-1 structure through a change in the χ_1 angle of residue 210 from approximately 69° to 168° (Figure 8). For the remaining changes, the reduction in available contact surface for the ligands with Asn175 (stromelysin-1) versus Gly175 (gelatinase-A) would lead to reduced favorable van der

Waals interactions of the compounds with gelatinase-A, while the minor Tyr to Phe swap at position 168 probably has little effect.

Conclusion

In this study we have used computational methods to estimate the free energy of binding for six ligands with stromelysin-1 and gelatinase-A using GB-MD simulations and MM-GBSA analysis. The predicted and experimental binding affinities ($\Delta G_{MM\text{-}GBSA}$) show strong correlation (Figure 8, $r^2 = 0.71$) which provides support for using continuum MD simulations, as an alternative to explicit water based simulations, to generate the snapshots used in subsequent MM-PBSA/GBSA analysis. Convergence of the GB-MD simulations was carefully monitored through examination of instantaneous computed free energies of binding, and individual energy components (Figure 3). Despite the short simulation times, all structural and energetic properties attributed to the GB-MD simulations appear to be well converged. A limitation of the present method is that, unlike simulations containing explicit water, detailed solute-solvent interactions are absent. However, continuum methods are expected to have an added utility where increased sampling is desired and/or computational expense is of concern.

$\Delta G_{MM\text{-}GBSA}$ results contain terms representing the average intermolecular protein-ligand coulombic and van der Waals energies (MM term), as well as a solvation term equivalent to the change in free energy of hydration for the system (GBSA term) upon complex formation. Interestingly, inclusion of solute entopic estimates ($\Delta G_{MM\text{-}GBSA+E}$) improved the correlation for the ligands with stromelysin-1 but diminished the correlation for the ligands with gelatinase-A. Removal of the solute entropies improved the total

correlation, consisting of all ligands complexed with both receptor, slightly ($\Delta G_{MM\text{-}GBSA}$, $r^2 = 0.74$ versus $\Delta G_{MM\text{-}GBSA+E}$, $r^2 = 0.71$).

In all cases, the simulation results correctly predict that a given ligand will bind selectively to stromelysin-1 rather than gelatinase-A (Figure 6). Selectivity appears to be dominated by; (1) increased favorable van der Waals interactions, (2) increased favorable coulombic interactions, and (3) decreased unfavorable total electrostatic energies ($\Delta E_{electro} = \Delta E_{coul} + \Delta G_{polar} + \Delta G_{nonpolar}$) for the ligands with stromelysin-1. A comparison of the protein residues that line the different binding pockets (Figures 7-8) in the simulations reveals that three aromatic rings make significant contact with each ligand in stromelysin-1 versus one aromatic ring in gelatinase-A. These changes probably account for the reduction in favorable protein-ligand interactions.

The highly complex and various roles that specific MMPs appear to play in various stages of tumor growth and metastasis represent a major challenge for the development of clinically effective chemotherapeutics. In this report, we have participated towards this goal by demonstrating that MM-GBSA simulation methods can be used to effectively model MMP-ligand complexes and that the simulation results can be used to make free energy of binding predictions that correlate strongly with experimental affinities. In particular, the correct selectivity trends for ligands with stromelysin-1 versus gelatinase-A were obtained. The fact that clinical trial results for first generation MMP inhibitors have been disappointing highlights the need for additional computational studies that continue to address selectivity.

Acknowledgment. Gratitude is expressed to Professor David A. Case, Kevin M. Masukawa, and Tiba Aynechi for helpful discussions, Jim Frazine for computational support, and to the Department of Defense for support of this research.

References

(1) Foda, H. D.; Zucker, S. Matrix metalloproteinases in cancer invasion, metastasis and angiogenesis. *Drug Discov. Today* **2001**, *6*, 478-482.

(2) Zucker, S.; Cao, J.; Chen, W. T. Critical appraisal of the use of matrix metalloproteinase inhibitors in cancer treatment. *Oncogene* **2000**, *19*, 6642-6650.

(3) Sternlicht, M. D.; Werb, Z. How matrix metalloproteinases regulate cell behavior. *Annu. Rev. Cell. Dev. Biol.* **2001**, *17*, 463-516.

(4) Whittaker, M.; Floyd, C. D.; Brown, P.; Gearing, A. J. H. Design and therapeutic application of matrix metalloproteinase inhibitors. *Chem. Rev.* **1999**, *99*, 2735-2776.

(5) Coussens, L. M.; Fingleton, B.; Matrisian, L. M. Matrix metalloproteinase inhibitors and cancer: trials and tribulations. *Science* **2002**, *295*, 2387-2392.

(6) Cornelius, L. A.; Nehring, L. C.; Harding, E.; Bolanowski, M.; Welgus, H. G.; Kobayashi, D. K.; Pierce, R. A.; Shapiro, S. D. Matrix metalloproteinases generate angiostatin: effects on neovascularization. *J. Immunol* **1998**, *161*, 6845-6852.

(7) O'Reilly, M. S.; Wiederschain, D.; Stetler-Stevenson, W. G.; Folkman, J.; Moses, M. A. Regulation of angiostatin production by matrix metalloproteinase-2 in a model of concomitant resistance. *J. Biol. Chem.* **1999**, *274*, 29568-29571.

(8) Purcell, W. T.; Rudek, M. A.; Hidalgo, M. Development of matrix metalloproteinase inhibitors in cancer therapy. *Hematol. Oncol. Clin. North. Am.* **2002**, *16*, 1189-1227.

(9) Overall, C. M.; Lopez-Otin, C. Strategies for MMP inhibition in cancer: innovations for the post-trial era. *Nat. Rev. Cancer* **2002**, *2*, 657-672.

(10) Hidalgo, M.; Eckhardt, S. G. Development of matrix metalloproteinase inhibitors in cancer therapy. *J. Natl. Cancer Inst.* **2001**, *93*, 178-193.

(11) Kuntz, I. D. Structure-based strategies for drug design and discovery. *Science* **1992**, *257*, 1078-1082.

(12) Jacobsen, E. J.; Mitchell, M. A.; Hendges, S. K.; Belonga, K. L.; Skaletzky, L. L.; Stelzer, L. S.; Lindberg, T. J.; Fritzen, E. L.; Schostarez, H. J.; O'Sullivan, T. J.; Maggiora, L. L.; Stuchly, C. W.; Laborde, A. L.; Kubicek, M. F.; Poorman, R. A.; Beck, J. M.; Miller, H. R.; Petzold, G. L.; Scott, P. S.; Truesdell, S. E.; Wallace, T. L.; Wilks, J. W.; Fisher, C.; Goodman, L. V.; Kaytes, P. S.; et al. Synthesis of a series of stromelysin-selective thiadiazole urea matrix metalloproteinase inhibitors. *J. Med. Chem.* **1999**, *42*, 1525-1536.

(13) Garbett, E. A.; Reed, M. W.; Stephenson, T. J.; Brown, N. J. Proteolysis in human breast cancer. *Mol. Pathol.* **2000**, *53*, 99-106.

(14) Bartsch, J. E.; Staren, E. D.; Appert, H. E. Matrix metalloproteinase expression in breast cancer. *J. Surg. Res.* **2003**, *110*, 383-392.

(15) Finzel, B. C.; Baldwin, E. T.; Bryant, G. L., Jr.; Hess, G. F.; Wilks, J. W.; Trepod, C. M.; Mott, J. E.; Marshall, V. P.; Petzold, G. L.; Poorman, R. A.; O'Sullivan, T. J.; Schostarez, H. J.; Mitchell, M. A. Structural characterizations of nonpeptidic

thiadiazole inhibitors of matrix metalloproteinases reveal the basis for stromelysin selectivity. *Protein Sci.* **1998**, *7*, 2118-2126.

(16) Dhanaraj, V.; Williams, M. G.; Ye, Q.-Z.; Molina, F.; Johnson, L. L.; Ortwine, D. F.; Pavlovsky, A.; Rubin, J. R.; Skeean, R. W.; White, A. D.; Humblet, C.; Hupe, D. J.; Blundell, T. L. X-Ray Structure of Gelatinase a Catalytic Domain Complexed with a Hydroxamate Inhibitor. *Croatica Chemica Acta* **1999**, *72*, 575-591.

(17) Sternlicht, M. D.; Lochter, A.; Sympson, C. J.; Huey, B.; Rougier, J. P.; Gray, J. W.; Pinkel, D.; Bissell, M. J.; Werb, Z. The stromal proteinase MMP3/stromelysin-1 promotes mammary carcinogenesis. *Cell* **1999**, *98*, 137-146.

(18) Sternlicht, M. D.; Bissell, M. J.; Werb, Z. The matrix metalloproteinase stromelysin-1 acts as a natural mammary tumor promoter. *Oncogene* **2000**, *19*, 1102-1113.

(19) Gohlke, H.; Klebe, G. Approaches to the description and prediction of the binding affinity of small-molecule ligands to macromolecular receptors. *Angew. Chem. Int. Ed. Engl.* **2002**, *41*, 2644-2676.

(20) Srinivasan, J.; Cheatham, T. E.; Cieplak, P.; Kollman, P. A.; Case, D. A. Continuum solvent studies of the stability of DNA, RNA, and phosphoramidate - DNA helices. *J. Am. Chem. Soc.* **1998**, *120*, 9401-9409.

(21) Kollman, P. A.; Massova, I.; Reyes, C.; Kuhn, B.; Huo, S.; Chong, L.; Lee, M.; Lee, T.; Duan, Y.; Wang, W.; Donini, O.; Cieplak, P.; Srinivasan, J.; Case, D. A.; Cheatham, T. E. Calculating structures and free energies of complex molecules:

combining molecular mechanics and continuum models. *Acc. Chem. Res.* **2000**, *33*, 889-897.

(22) Massova, I.; Kollman, P. A. Combined molecular mechanical and continuum solvent approach (MM-PBSA/GBSA) to predict ligand binding. *Perspect. Drug Discov. Design* **2000**, *18*, 113-135.

(23) Åqvist, J.; Medina, C.; Samuelsson, J.-E. A New Method For Predicting Binding Affinity in Computer-Aided Drug Design. *Protein Eng.* **1994**, *7*, 385-391.

(24) Rizzo, R. C.; Tirado-Rives, J.; Jorgensen, W. L. Estimation of Binding Affinities for HEPT and Nevirapine Analogues with HIV-1 Reverse Transcriptase via Monte Carlo Simulations. *J. Med. Chem.* **2001**, *44*, 145-154.

(25) Pierce, A. C.; Jorgensen, W. L. Estimation of Binding Affinities for Selective Thrombin Inhibitors via Monte Carlo Simulations. *J. Med. Chem.* **2001**, *44*, 1043-1050.

(26) Rizzo, R. C.; Udier-Blagovic, M.; Wang, D. P.; Watkins, E. K.; Kroeger Smith, M. B.; Smith, R. H., Jr.; Tirado-Rives, J.; Jorgensen, W. L. Prediction of activity for nonnucleoside inhibitors with HIV-1 reverse transcriptase based on Monte Carlo simulations. *J. Med. Chem.* **2002**, *45*, 2970-2987.

(27) Wesolowski, S. S.; Jorgensen, W. L. Estimation of binding affinities for celecoxib analogues with COX-2 via Monte Carlo-extended linear response. *Bioorg. Med. Chem. Lett.* **2002**, *12*, 267-270.

(28) Donini, O. A. T.; Kollman, P. A. Calculation and prediction of binding free energies for the matrix metalloproteinases. *J. Med. Chem.* **2000**, *43*, 4180-4188.

(29) Kuhn, B.; Kollman, P. A. Binding of a diverse set of ligands to avidin and streptavidin: An accurate quantitative prediction of their relative affinities by a combination of molecular mechanics and continuum solvent models. *J. Med. Chem.* **2000**, *43*, 3786-3791.

(30) Wang, J.; Morin, P.; Wang, W.; Kollman, P. A. Use of MM-PBSA in reproducing the binding free energies to HIV-1 RT of TIBO derivatives and predicting the binding mode to HIV-1 RT of efavirenz by docking and MM-PBSA. *J. Am. Chem. Soc.* **2001**, *123*, 5221-5230.

(31) Masukawa, K. M.; Kollman, P. A.; Kuntz, I. D. Investigation of Neuraminidase-Substrate Recognition Using Molecular Dynamics and Free Energy Calculations. *J. Med. Chem.* **2003**, *46*, 5628-5637.

(32) Huo, S.; Wang, J.; Cieplak, P.; Kollman, P. A.; Kuntz, I. D. Molecular dynamics and free energy analyses of cathepsin D-inhibitor interactions: insight into structure-based ligand design. *J. Med. Chem.* **2002**, *45*, 1412-1419.

(33) Wang, W.; Lim, W. A.; Jakalian, A.; Wang, J.; Luo, R.; Bayly, C. I.; Kollman, P. A. An analysis of the interactions between the Sem-5 SH3 domain and its ligands using molecular dynamics, free energy calculations, and sequence analysis. *J. Am. Chem. Soc.* **2001**, *123*, 3986-3994.

(34) Suenaga, A.; Hatakeyama, M.; Ichikawa, M.; Yu, X.; Futatsugi, N.; Narumi, T.; Fukui, K.; Terada, T.; Taiji, M.; Shirouzu, M.; Yokoyama, S.; Konagaya, A. Molecular dynamics, free energy, and SPR analyses of the interactions between the SH2 domain of Grb2 and ErbB phosphotyrosyl peptides. *Biochemistry* **2003**, *42*, 5195-5200.

(35) *MOE Version 2002.03*; Chemical Computing Group: Montreal, Canada.

(36) Wang, J. M.; Cieplak, P.; Kollman, P. A. How well does a restrained electrostatic potential (RESP) model perform in calculating conformational energies of organic and biological molecules? *J. Comput. Chem.* **2000**, *21*, 1049-1074.

(37) Stote, R. H.; Karplus, M. Zinc binding in proteins and solution: a simple but accurate nonbonded representation. *Proteins* **1995**, *23*, 12-31.

(38) *AMBER Version 7*; University of California at San Francisco: San Francisco, CA.

(39) Vaz, R. J.; Kuntz, I. D.; Meng, E. C. Evaluating non-bonded parameters for zinc in DOCK. *Med. Chem. Res.* **1999**, *9*, 479-489.

(40) Jakalian, A.; Bush, B. L.; Jack, D. B.; Bayly, C. I. Fast, efficient generation of high-quality atomic charges. AM1- BCC model: I. Method. *J. Comput. Chem.* **2000**, *21*, 132-146.

(41) Jakalian, A.; Jack, D. B.; Bayly, C. I. Fast, efficient generation of high-quality atomic charges. AM1-BCC model: II. Parameterization and validation. *J. Comput. Chem.* **2002**, *23*, 1623-1641.

(42) Hawkins, G. D.; Cramer, C. J.; Truhlar, D. G. Pairwise Solute Descreening of Solute Charges from a Dielectric Medium. *Chem. Phys. Lett.* **1995**, *246*, 122-129.

(43) Hawkins, G. D.; Cramer, C. J.; Truhlar, D. G. Parametrized models of aqueous free energies of solvation based on pairwise descreening of solute atomic charges from a dielectric medium. *J. Phys. Chem.* **1996**, *100*, 19824-19839.

(44) Berendsen, H. J. C.; Postma, J. P. M.; Vangunsteren, W. F.; Dinola, A.; Haak, J. R. Molecular-Dynamics with Coupling to an External Bath. *J. Chem. Phys.* **1984**, *81*, 3684-3690.

(45) Ryckaert, J. P.; Ciccotti, G.; Berendsen, H. J. C. Numerical-Integration of Cartesian Equations of Motion of a System with Constraints - Molecular-Dynamics of N-Alkanes. *J. Comput. Phys.* **1977**, *23*, 327-341.

(46) Sitkoff, D.; Sharp, K. A.; Honig, B. Accurate Calculation of Hydration Free-Energies Using Macroscopic Solvent Models. *J. Phys. Chem.* **1994**, *98*, 1978-1988.

(47) Tsui, V.; Case, D. A. Molecular dynamics simulations of nucleic acids with a generalized born solvation model. *J. Am. Chem. Soc.* **2000**, *122*, 2489-2498.

(48) Thompson, J. D.; Higgins, D. G.; Gibson, T. J. Clustal W: Improving the Sensitivity of Progressive Multiple Sequence Alignment through Sequence Weighting, Position-Specific Gap Penalties and Weight Matrix Choice. *Nucleic Acids Res.* **1994**, *22*, 4673-4680.

(49) BOXSHADE Version 3.21; http://www.ch.embnet.org/software/BOX_form.html.